Chemical Science

rsc.li/chemical-science

ROYAL SOCIETY OF CHEMISTRY

EDGE ARTICLE

Muzzamil Ahmad Eatoo and Himanshu Mishra
Busting the myth of spontaneous formation of H_2O_2 at the air–water interface: contributions of the liquid–solid interface and dissolved oxygen exposed

EDGE ARTICLE

Check for updates

All publication charges for this article have been paid for by the Royal Society of Chemistry

Busting the myth of spontaneous formation of H$_2$O$_2$ at the air–water interface: contributions of the liquid–solid interface and dissolved oxygen exposed†

Muzzamil Ahmad Eatoo [ID] [ab] and Himanshu Mishra [ID] *[abc]

Recent reports on the spontaneous formation of hydrogen peroxide (H$_2$O$_2$) at the air–water and solid–water interfaces challenge our current understanding of aquatic chemistry and have ramifications on atmosphere chemistry models, surface science, and green chemistry. Suggested mechanisms underlying this chemical transformation include ultrahigh instantaneous electric fields at the air–water interface and the oxidation of water and reduction of the solid at the solid–water interface. Here, we revisit this curious problem with NMR spectroscopy (with an H$_2$O$_2$ detection limit ≥50 nM) and pay special attention to the effects of nebulizing gas, dissolved oxygen content, and the solid–water interface on this chemical transformation in condensed and sprayed water microdroplets. Experiments reveal that the reduction of dissolved oxygen at the solid–water interface predominantly contributes to the H$_2$O$_2$ formation (not the oxidation of hydroxyl ions at the air–water interface or the oxidation of water at the solid–water interface). We find that the H$_2$O$_2$ formation is accompanied by the consumption (*i.e.*, reduction) of dissolved oxygen and the oxidation of the solid surface, *i.e.*, in the absence of dissolved oxygen, the formation of H$_2$O$_2$(aq) is not observed within the detection limit of ≥50 nM. Remarkably, the tendency of the solids investigated in this work towards forming H$_2$O$_2$ in water followed the same order as their positions in the classic Galvanic series. These findings bust the prevailing myths surrounding H$_2$O$_2$ formation due to the air–water interface, the ultrahigh electric fields therein, or the micro-scale of droplets. The hitherto unrealized role of the oxidation of the solid surface due to dissolved oxygen in the formation of H$_2$O$_2$ is exposed. These findings are especially relevant to corrosion science, surface science, and electrochemistry, among others.

Introduction

Hydrogen peroxide (H$_2$O$_2$) is an industrial chemical with a wide range of applications, such as disinfection,[1] chemical synthesis,[2] rocket propulsion,[3] and wastewater treatment.[4] The current production of H$_2$O$_2$ at scale relies on the anthraquinone cycling process, requiring significant energy and generating waste,[5] necessitating sustainable alternatives. Recent reports on the laboratory-scale production of H$_2$O$_2$ *via* electrochemical oxygen reduction are promising.[6–8] However, electrochemical

[a]Environmental Science and Engineering (EnSE) Program, Biological and Environmental Science and Engineering (BESE) Division, King Abdullah University of Science and Technology (KAUST), 23955-6900, Thuwal, Kingdom of Saudi Arabia

[b]Water Desalination and Reuse Center (WDRC), King Abdullah University of Science and Technology (KAUST), 23955-6900, Thuwal, Kingdom of Saudi Arabia. E-mail: Himanshu.Mishra@kaust.edu.sa

[c]Center for Desert Agriculture (CDA), King Abdullah University of Science and Technology (KAUST), 23955-6900, Thuwal, Kingdom of Saudi Arabia

† Electronic supplementary information (ESI) available. See DOI: https://doi.org/10.1039/d3sc06534k

methods are not devoid of shortcomings; the process is complex and has the risk of spontaneous combustion and explosion. Multiple side reactions may further restrict the scalability of the process.

In this context, sensational reports on the spontaneous formation of H$_2$O$_2$ at the aerial interface of water microdroplets seem enticing.[9–13] Specifically, about 30 μM H$_2$O$_2$ was found in water microdroplets with a diameter of ≤20 μm sprayed *via* pressurized gas,[9] and ≤115 μM H$_2$O$_2$ was discovered in condensed water microdroplets on common substrates in the relative humidity range of 40% to 70%.[10] The presence of ultrahigh electric fields on microdroplet surfaces has been speculated to be the underlying cause.[9,10] Moreover, studies have noted the implications for atmospheric chemistry,[14] human health and bactericidal applications,[13] green chemistry,[9,14] and the seasonality of diseases due to the Goldilocks effect.[12,15] We introduce the investigation of this chemical transformation by noting that the examination of water's interfaces is notorious for artifacts arising from contamination, incorrect interpretations of experiments, and the lack of

encompassing multiscale computational models.[16–38] Experience in microdroplet chemistry has demonstrated the need to stress-test the conclusion *via* multiple experimental techniques.

The prospect of aerosolized water microdroplets producing H_2O_2 is appealing due to its greenness and potential ease of application.[13,39] While some experiments,[40–43] computer simulations,[44,45] and a Gedankenexperiment[46] have given credence to the claim of spontaneous H_2O_2 formation at the air–water interface, others have disagreed.[47–54] We commenced the investigation in 2019 by comparing the various commercially available assays for H_2O_2(aq). Compared to the potassium titanium oxalate assay (PTO; detection limit ≥ 10 μM), used in the original reports,[9,10] the hydrogen peroxide assay kit (HPAK) affords a 40-times lower detection limit (≥ 250 nM). Equipped with HPAK, we employed a glovebox to assess H_2O_2(aq) concentrations in condensed water microdroplets generated in an N_2(g) environment by gently heating water (50–70 °C). This experiment revealed that the H_2O_2 concentrations in the bulk water and the condensates were indistinguishable.[47] We also discovered that if the condensates were produced *via* ultrasonic humidifiers, about 1 μM H_2O_2(aq) was produced in the water reservoir, the mist, and the condensates.[47] This result was rationalized on the basis of the cavitating bubbles formed under ultrasonic acoustic pressure in bulk water, which is known to produce OH• radicals.[49,55–58] However, why Zare & co-workers found ≤ 115 μM H_2O_2 in their experiments remained unclear.

From 2020 to 2021, we broadened the investigation to include microdroplets produced by pneumatic sprays. This device, like the one in the original report,[9] facilitated the gas flow speeds of 100 to 1000 ms^{-1}, breaking up water droplets to form sprays. In all these studies, (i) sprayed water microdroplets were collected in glass bottles, and (ii) condensed microdroplets were formed on SiO_2/Si wafers. We discovered that the ppm-level of spontaneous H_2O_2 formation (1 ppm = 29.4 μM H_2O_2) occurred only in the presence of ozone (O_3(g)).[48]

In their latest report, Zare & co-workers[59] repeated the spray experiments in a controlled (ozone-free) gas environment. They employed ^{1}H-NMR to quantify H_2O_2(aq) at a 40 nM resolution following the protocol of Bax *et al.* (Bruker 600 MHz Avance III, noncryogenic probe, 20 000 scans with 0.1 s acquisition time).[41,60] When the water was injected through copper tubing in the flow rate range of 25 to 150 μL min^{-1} *via* a pressurized N_2 at 100 psi (6.8 atm), the H_2O_2(aq) concentration in the sprays ranged from 1.5 to 0.3 μM (95–99% reduction from the original report[9]). They also found that, for a fixed liquid flow rate, as the nebulizing gas (fixed line pressure) was changed from (i) N_2 to (ii) $N_2 + O_2$ (2%) to (iii) $N_2 + O_2$ (21%) to (iv) O_2 (100%), the H_2O_2(aq) concentration increased from (i) 0.49 ± 0.05 μM to (ii) 0.69 ± 0.05 μM to (iii) 1.12 ± 0.02 μM to (iv) 2.00 ± 0.05 μM, respectively.[59] Based on these observations, they contend that their original claims were correct (*i.e.*, the microdroplet air–water interface spontaneously produces H_2O_2).

Even if we assume that the latest claim is valid, the previous reports,[9,10] which applied the PTO assay (H_2O_2 detection limit ≥ 10 μM), could not have detected the 0.30 to 2.00 μM H_2O_2(aq) concentrations (*i.e.*, they were reporting artifacts of the ambient

ozone gas[48]). This admission may help explain the latest[59] and previous[9] reports by Zare & co-workers of contradictory trends in the H_2O_2(aq) concentrations in water microdroplets when the concentration of dissolved oxygen (O_2(aq)) is increased (explained in concluding remarks).

Lastly, two new experimental reports have surfaced in which H_2O_2 formation is also observed at the silica–water interface when (i) liquid water passes through a polydimethylsiloxane microfluidic chip placed on glass,[11] and (ii) water vapor passes through a packed bed of SiO_2 nanoparticles.[15] Regarding the mechanism, the authors stated, "In fact, our proposed mechanism is built around the hypothesis that the overlap between the electron clouds of the water molecule and the solid surface during the contact will lead to the generation of H_2O^+ and OH•".[11] They also presented an example: "Then, the electron may transfer from the water molecule to the surface of SiO_2, which is the so-called contact electrification".[15]

In this contribution, we investigate whether the skin of water (the air–water interface) is so unstable that airborne microdroplets can spontaneously produce H_2O_2, or whether another process is occurring. We investigate the origins of approx. 1 μM H_2O_2 in condensed and sprayed water microdroplets *via* ^{1}H-NMR, to answer the following interrelated fundamental questions:

(1) Is H_2O_2 formation in water microdroplets influenced by the nature of the nebulizing gas (*viz.*, N_2 or O_2)?

(2) Would the H_2O_2 concentration in condensates collected in an inert gaseous environment be the same or different if the solid surface composition is varied (*e.g.*, a SiO_2/Si wafer or stainless steel)?

(3) Is the 'micro' scale of droplets necessary for the spontaneous formation of H_2O_2 at aqueous interfaces? What would the result be if pellets of a solid material (*e.g.*, aluminum or mild steel) were immersed in bulk water, or if a film of water was sandwiched between two solid surfaces to eliminate the air–water interface from the picture?

(4) What is the role of dissolved oxygen (in water) in this chemical transformation? If the dissolved oxygen were removed from the water and sprayed, would H_2O_2 still form?

(5) During the spontaneous H_2O_2 formation at the solid–water interface, do water molecules transfer electrons to the solid and therefore reduce it?[11,15]

(6) Which aqueous interface would produce more H_2O_2 for a fixed area: the air–water interface or the solid–water interface (solid refers to common materials, such as glass, steel, *etc.*)?

Results

In a controlled gaseous environment (N_2(g), unless specified otherwise) afforded by a clean glovebox, we collected water microdroplets formed *via* pneumatic sprays (Fig. S1 and Section S1 present the details†) or by condensing the vapor generated by gently heating water (60 °C) onto cold surfaces. First, we probed the effects of the nebulizing gas (N_2 or O_2) on the H_2O_2(aq) concentration. We applied the flow rates suggested by Zare & co-workers[59] to maximize the H_2O_2 formation: a water flow rate of 25 μL min^{-1} through a 0.10 mm-wide silica capillary, nebulizing

Fig. 1   Pneumatic spraying of water into microdroplets produces H_2O_2. (a) Illustration of the experimental setup: as the nebulizing gas changes from $N_2(g)$ to $O_2(g)$, the $H_2O_2(aq)$ concentration increases from 1.0 ± 0.2 μM to 3.0 ± 0.2 μM. (b) Representative ^{1}H-NMR spectra of the reference standard, 1 μM H_2O_2 solution (red); ^{1}H-NMR spectra of $H_2O_2(aq)$ in water microdroplets nebulized by high pressure (100 psi) N_2 (blue) and O_2 (green) gases at an injection rate of 25 μL min^{-1}. A description of our experimental set up is presented in ESI Section S1† along with photographs (Fig. S1†).

$N_2(g)$ gas at 100 psi shearing through an outer concentric tube of 0.43 mm in diameter (Fig. 1a & S1†). The spray was collected in a custom-built glass container, as described previously[48] (Fig. S1†). The quantification of $H_2O_2(aq)$ relied on ^{1}H-NMR *via* the remarkable protocol of Bax *et al.*,[60] which was also followed by Zare & co-workers.[41,59] We employed a Bruker 950 MHz Avance Neo NMR spectrometer equipped with a 5 mm *Z*-axis gradient TCI cryoprobe at 275 K. During each measurement, a 6 ms Gaussian 90° pulse was applied to selectively excite the protons of H_2O_2, followed by a 53 ms acquisition time corresponding to 1024 detection points with a spectral width of 9615 Hz. Over 50 000 scans were collected with a recycle delay of 1 ms between the scans. With this technique, we observed $H_2O_2(aq)$ down to approx. 50 nM detection limit (see Fig. S2† for a representative calibration plot).

The ^{1}H-NMR results confirmed the presence of 1.0 ± 0.2 μM H_2O_2 in water microdroplets sprayed using N_2 gas (Fig. 1). Next, when we switched the nebulizing gas to O_2, keeping the water flow the same, the H_2O_2 concentration increased to 3.0 ± 0.2 μM (Fig. 1). Two crucial questions arose, which we address next: (i) If this phenomenon is driven by an ultrahigh instantaneous electric field at the air–water interface, then why does the nebulizing gas influence it; (ii) Could the solid–water interface drive this chemical transformation?

To answer these questions, we compared the amount of $H_2O_2(aq)$ formed in water microdroplets condensed onto a variety of smooth and flat substrates: SiO$_2$/Si wafers, polished titanium, polished stainless steel (SS304), polished mild steel, silicon surfaces (obtained by the reactive ion etching of SiO$_2$/Si wafers), polished copper (Cu), polished magnesium alloy (Mg alloy, AZ31B), and polished aluminum (Al) (see Methods for details). Mechanical polishing was performed using emery paper with a grit size ranging from 400 to 1500 to remove the native oxide layer. While the size distribution of the microdroplets formed on these substrates did not vary significantly

because of their superhydrophilic nature, a dramatic difference in the amount of $H_2O_2(aq)$ occurred in the condensates, depending on the nature of the substrate (Fig. 2). For instance, as we replaced the SiO$_2$/Si wafer substrate with a Mg alloy (AZ31B), the H_2O_2 concentration rose from 0.4 ± 0.2 μM to 68 ± 5 μM (Fig. 2). In this four year-long investigation of this phenomenon, predominantly with null results, this was the first time we observed the formation of ppm-level H_2O_2 (aq) in water microdroplets in the absence of $O_3(g)$.

Notably, the H_2O_2 concentrations reported in Fig. 2 were those obtained on freshly prepared surfaces (*i.e.*, without a native oxide layer). Over time, as the condensation experiments were repeated on the same surface, the extent of the $H_2O_2(aq)$ formation decreased, underscoring the importance of the solid–water interface. For instance, the H_2O_2 produced on a freshly prepared Al surface was around 30 to 35 μM, which decreased to 7 to 8 μM in the second cycle and to 4 to 5 μM in the third cycle (each separated by 10 min).

Having identified that microdroplets placed on common materials, such as (polished) aluminum, produce ppm-level H_2O_2, we assessed the importance of the droplet size in this chemical transformation. We formed a 1 : 1 volumetric solution of deionized (DI) water with the HPAK reaction mixture and placed a macroscopic 1000 μL droplet (a base diameter of 12 000 μm) onto an Al plate. Within a few seconds, we observed a sharp blue fluorescence – proof of the formation of $H_2O_2(aq)$ – with an unambiguous gradient emanating from the Al–water interface (Fig. 3 and ESI Movie 1†). Judging by the fluorescence intensity, the local concentration of $H_2O_2(aq)$ at the solid–liquid interface is at the ppm level (*i.e.*, the air–water interface produced no fluorescence visible to the naked eye).

Building on this experiment, we reduced the air–water interfacial area from this three-phase system by (i) layering 1 ml of fresh DI-water–HPAK 1 : 1 mixture between two 20 × 20 cm^2 Al plates and (ii) immersing freshly polished Mg pellets (6.2
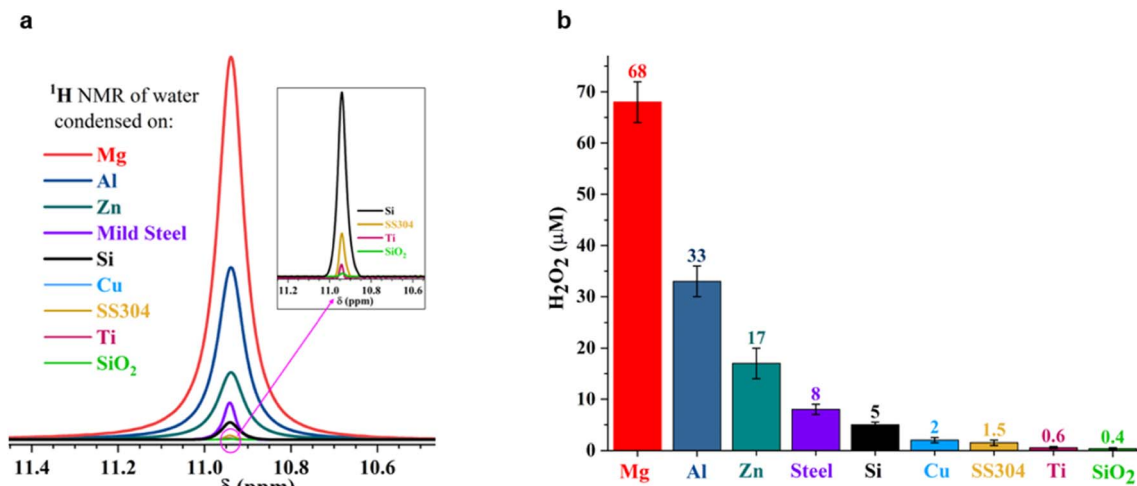
Fig. 2 Concentration of $H_2O_2(aq)$ formed in condensed water microdroplets varies with the nature of the solid substrate. (a) Selective-excitation ^1H-NMR spectra for H_2O_2 quantification following the protocols developed by Bax et al.[60] (b) Measured $H_2O_2(aq)$ concentrations in condensates collected from the various substrates varied by over two orders of magnitude, confirmed via ^1H-NMR and HPAK. The air–water interfacial area of the microdroplets was not too dissimilar in these scenarios; thus, the solid–water interface drives the formation of H_2O_2.

cm^2) in 5 ml of bulk DI water–HPAK 1 : 1 mixture (Fig. 4c and d). In all these scenarios, we discovered that the solid–water interface was the site for the spontaneous H_2O_2 formation, and the air–water interface had a negligible effect, if any. This observation is based on the distinct color gradient at the solid–water interface. After these experiments, we collected the water samples (films or bulk) and took ^1H-NMR measurements (Table S1†). The H_2O_2 concentration produced by a sessile water droplet (~1 ml) placed on a freshly polished Al plate and the scenarios (i) and (ii) listed above after 1 minute was 1.4 ± 0.5 μM, 39 ± 6 μM, and 2.5 ± 0.6 μM, respectively. A systematic study of the effects of the solid–water surface area and the effect of time is underway. These results unambiguously establish that the spontaneous H_2O_2 production in water does not necessitate microscopic droplets or the air–water interface, and it can occur even in bulk water when specific solid materials are introduced.

Next, we probed the surfaces before and after contact with water via X-ray photoelectron spectroscopy (XPS), which revealed that the spontaneous H_2O_2 formation at the water-solid surface was accompanied by substrate oxidation. For instance, on contact with water (condensed or both), metallic Al (Al^0) was oxidized to Al^{3+}, and semiconductor silicon (Si^0) was oxidized to the Si^{4+} oxidation state (Fig. 5a–c). The water microdroplets spread and merged during each cycle, covering the entire (superhydrophilic) solid surface by the end of each cycle. This finding contradicts the claims that during H_2O_2 formation at the solid–water interface, OH^- ions are oxidized to $OH^·$ (or H_2O molecules are oxidized to H_2O^+),[11,15] because, if this were true, the solid surface would be getting reduced, which is not the case. An in depth characterization of oxidation products is beyond the scope of this study and will be explored in the future.

Following the XPS study, we noticed that the H_2O_2 formation was accompanied by surface oxidation. Therefore, we got curious whether it was due to the reduction of the dissolved oxygen.[61] To examine this, we first removed dissolved O_2 from the water by heating it in an autoclave to its boiling point, followed by $N_2(g)$ bubbling for 45 minutes and then sealing it inside an N_2-purged container (methods). This treatment

Fig. 3 Time-dependent formation of $H_2O_2(aq)$ in a macroscopic droplet of a 1 : 1 mixture of water and HPAK reaction mixture on an Al plate (see ESI Movie S1†). Within seconds, $H_2O_2(aq)$ formation at the Al–water interface is evident, proving that the size of the droplet and air–water interface do not matter. The solid–water interface drives this chemical transformation. The Al surface is superhydrophilic, and water spreads on it as a film. Therefore, the Al plate was placed vertically on a polystyrene sheet and formed a 1 ml droplet resting on the Al edge. The 1 : 1 mixture of water and HPAK reaction on polystyrene did not yield the faintest blue fluorescence visible to the naked eye.

Fig. 4 Illustration capturing the experimental observations: (a) No H_2O_2 is formed in the water microdroplets suspended in the air (*i.e.*, without any contact with a solid). (b) H_2O_2 formation in water microdroplets on a solid substrate. (c) H_2O_2 formation in a water film between two solids. (d) H_2O_2 formation in bulk water at the solid–water interface. In the latter two cases, the air–water interface was practically eliminated. See text above and Table S1† for experimental details.

reduced the $O_2(aq)$ concentration to <0.01 mg L^{-1}. Microdroplets of O_2-free water were formed *via* pneumatic spraying using $N_2(g)$ in an N_2 environment and collected in glass containers (following the same protocol). The $H_2O_2(aq)$ concentration was compared with that in the microdroplets formed with water containing dissolved $O_2(g)$ (Fig. 6a).

Fig. 5 Representative XPS analysis of freshly polished metallic surfaces before and after contact with water. (a) High-resolution spectra of Al 2p before the condensation of water reveal a dominant metallic Al^0 peak at 72.6 eV. After condensation cycles, the Al^0 peak shrinks while the oxidized Al^{3+} peak (at 75.4 eV) increases. (b) High-resolution spectra of Si 2p before the water condensation cycle reveal a Si^0 peak at 99.7 eV. After a water condensation cycle, the Si^0 peak shrinks, and the Si^{4+} peak at 103.5 eV increases. (c) High-resolution XPS spectra of the O 1s peak on a freshly etched Si surface before and after a water condensation cycle. The surface oxygen composition increases from 9.0% to 50.7% after a condensation cycle due to the formation of the oxide layer.

Fig. 6 Role of the dissolved oxygen (O_2) in water in the formation of H_2O_2 in microdroplets and bulk forms. (a) An illustration of the experiments in which water containing dissolved O_2 and deoxygenated water was sprayed to form microdroplets. The microdroplets were collected in a glass vial, and $H_2O_2(aq)$ was quantified. (b) Within a detection limit of 50 nM, ^{1}H-NMR revealed that no H_2O_2 formed in the deoxygenated water, whereas $H_2O_2(aq)$ was readily detected in the presence of dissolved O_2. The air–water interface was common in both scenarios; thus, these experiments prove that the $H_2O_2(aq)$ formation happens at the solid–water interface and dissolved $O_2(aq)$ is the limiting factor. (c) In another experiment, we prepared a 1:1 mixture of the HPAK reaction mixture with deoxygenated water and for the control case prepared the mixture with water containing dissolved $O_2(aq)$. Next, H_2O_2 formation in the following three scenarios was investigated: (i) an Mg pellet was added to the 1:1 mixture saturated with the ambient $O_2(g)$ and the vial was exposed to the ambient air (*i.e.*, unlimited oxygen case); (ii) an Mg pellet was added to the 1:1 mixture saturated with dissolved oxygen $O_2(g)$, and the vial was sealed (*i.e.*, the limited oxygen case); and (iii) a pellet was added to the 1:1 mixture without dissolved $O_2(aq)$, and the vial was sealed (*i.e.*, the without O_2 case). In the absence of dissolved $O_2(aq)$, no $H_2O_2(aq)$ formed within the detection limit of 0.25 μM, whereas it appeared readily in the presence of $O_2(aq)$, demonstrating that this chemical transformation occurs at the solid–water interface and that dissolved $O_2(aq)$ is a reactant. Therefore, H_2O_2 formation is not a property of the air–water interface or dependent on the size of the droplets. (Scale bar: the diameter of the pellet is 1 cm).

Remarkably, in the absence of $O_2(aq)$, no $H_2O_2(aq)$ was observed *via* 1H-NMR (detection limit ≥50 nM; Fig. 6b). Next, we tested the effects of dissolved $O_2(g)$ on the formation of $H_2O_2(aq)$ in bulk water by adding metallic pellets (Mg or Al). We tested the following three scenarios:

(i) An Mg pellet was added to water saturated with the ambient $O_2(g)$, and the vial was left open in an O_3-free ambient environment.

(ii) An Mg pellet was added to water saturated with ambient oxygen $O_2(g)$ and then sealed.

(iii) An Mg pellet was added to O_2-free water in an $N_2(g)$ environment and sealed.

The vial open to the ambient air had significantly higher $H_2O_2(aq)$ than that in the sealed vial containing water saturated with dissolved $O_2(g)$. Thus, the formation of H_2O_2 at the solid–water interface consumes dissolved $O_2(g)$ (*i.e.*, it is the limiting factor). We also characterized the consumption of the dissolved $O_2(g)$ before and after adding the pellets and found that it decreased over time (Fig. S4†). Notably, in the absence of dissolved $O_2(g)$, we did not observe $H_2O_2(aq)$ within the detection limit of 50 nM (Fig. 6b). These results unambiguously establish (i) the importance of dissolved $O_2(g)$ in this chemical transformation and that (ii) the air–water interface of microdroplets is incapable of forming H_2O_2.

Discussion

We draw together the results of this study and previous scientific reports to discuss the mechanisms underlying the formation of H_2O_2 in interfacial water (Fig. 7). The first finding is that the amount of $H_2O_2(aq)$ formed in water condensates (or sprayed microdroplets) depends only on the nature of the surface on which it is collected (Fig. 2 and 3). In other words, the air–water interface or the size of the microdroplets has no bearing on the $H_2O_2(aq)$ formation (Fig. 3, 4d, and S5†). For instance, as the air–water interface is reduced (or eliminated) from the picture, *via* layering water films between solid plates (Fig. 4c) (or by introducing solid pellets into bulk water) the formation of $H_2O_2(aq)$ remains unaffected (Fig. 4c, d and S5†). The second crucial finding is that if the dissolved O_2 is removed from the water, there is no evidence for $H_2O_2(aq)$ formation within the detection limit (Fig. 6a–c). This observation contradicts the suggested mechanism for $H_2O_2(aq)$ formation due to the charge transfer between positively (H_3O^+ rich) and negatively charged (OH^- rich) microdroplets.[42,46]

Next, the XPS results demonstrate that the formation of $H_2O_2(aq)$ is accompanied by the oxidation of the solid surface and the reduction of dissolved O_2 (Fig. 5). Fig. S4† illustrates how the absolute concentration of $O_2(aq)$ decreases during H_2O_2 formation. When we evaluated the various commercially available materials used in this study in terms of their ability to form $H_2O_2(aq)$ in (air-equilibrated) water, the trend followed the Galvanic series: Mg > Al > Zn > mild steel > Si > Cu > stainless steel (SS304) > Ti > SiO_2/Si wafer (Fig. 7). Therefore, these findings refute the previous speculations regarding the oxidation of OH^- ions to $OH^•$ (or the oxidation of H_2O to H_2O^+) and the reduction of the solid surface during the H_2O_2 formation at the solid–water interface.[11,15]

We postulate that the initiation of this chemistry involves the reduction of dissolved $O_2(aq)$ by the solid surface; that is, the
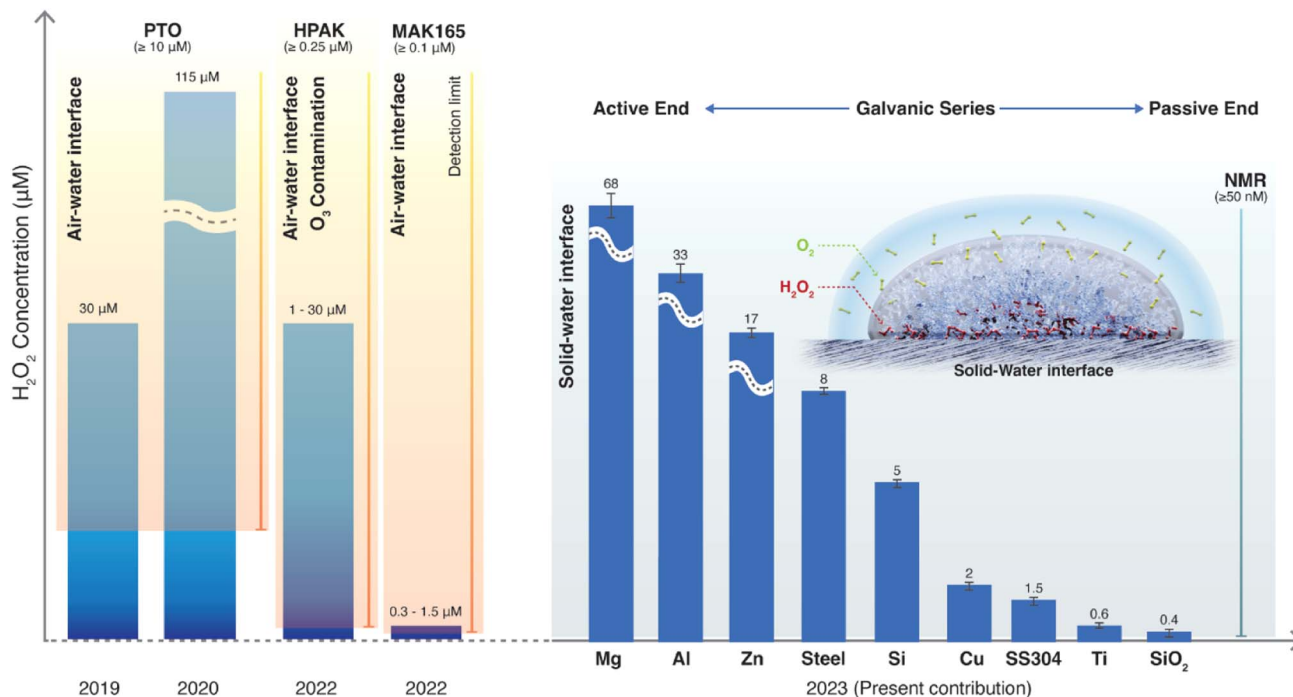
© 2024 The Author(s). Published by the Royal Society of Chemistry

Fig. 7 Current understanding of the spontaneous H_2O_2 formation in water microdroplets since its first report in 2019. Initial papers by Zare & coworkers used the PTO assay (detection limit $\geq$10 μM) and reported 30 and 110 μM H_2O_2(aq) in sprays and condensates, respectively.[9,10] In 2022, it was revealed that ambient O_3(g) could cause severe artifacts in these microdroplet experiments using HPAK (detection limit $\geq$0.25 μM).[48] In 2023, using ^{1}H-NMR (detection limit $\geq$0.04 μM), it was contended that in an O_3-free environment, the air–water interface still produces H_2O_2 ($\sim$1 μM).[59] In the present contribution using ^{1}H-NMR, we reveal that the solid–water interface is the site for H_2O_2(aq) formation, and the air–water interface does not contribute to H_2O_2 formation (quantified within the detection limit of $\geq$0.05 μM). If dissolved O_2 is removed from the water, H_2O_2(aq) is not observed within the detection limit. Next, depending on the nature of the substrate that water contacts (as microdroplets or a film or as bulk water), the amount of H_2O_2(aq) formed follows the classic Galvanic series.[62]

surface transfers two electrons into interfacial O_2(aq), transforming it into a highly reactive peroxide dianion ($O_2^{•2-}$).[63] We anticipate this anion species to hover near the solid–water interface due to electrostatic attraction. Next, the anion reacts with interfacial water molecules to form H_2O_2 and hydroxide ions[61,63] (the reactions below capture this logic):

$$O_2 + 2e^- \rightarrow O_2^{•2-} \tag{1}$$

$$O_2^{•2-} + 2H_2O \rightarrow H_2O_2 + 2OH^- \tag{2}$$
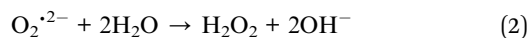
Reaction (2) indicates that the H_2O_2(aq) formation is accompanied by pH enhancement. The pH of the condensate collected on the Mg plate was around 7.9 ± 0.2, whereas the pH of the water reservoir used for gentle heating was 5.6 ± 0.1. The H_2O_2(aq) formation rate is the highest when the surface is free of native oxide and slows down as the oxide layer grows, which was also noticed in our experiments. Similar reaction schemes have been proposed recently, and in some of them, O_2 is the byproduct.[40] If this were true, then the H_2O_2(aq) formation due to the addition of a metal pellet (Mg or Al) to bulk water would be the same whether the dissolved O_2 content was (i) unlimited (Fig. 6ci), (ii) limited (Fig. 6cii) or (ii) nil (Fig. 6ciii), but that is not the case. An in-depth investigation of the reaction intermediates (Reactions (1) and (2)) and the contribution of metal pellets on water-splitting reactions and the water pH is underway.

Conclusion

These findings put to rest several myths surrounding the spontaneous formation of H_2O_2 at the air–water interface, including the instantaneous ultrahigh electric fields, the "microscale" of droplets,[9,10,12–14,40,41,44,45,59] and arguments based on charge transfer between microdroplets.[42,46] For water containing dissolved O_2, which is commonplace in environmental and applied scenarios, the solid–water interface is the site where O_2(aq) reduces and forms H_2O_2(aq). One can therefore expect trace level (<0.5 μM) H_2O_2 to be produced at (clean) glass–water interfaces in laboratories routinely that, depending on the surface-to-volume ratio, may impact ultrasensitive investigation of aqueous interfaces and engineering processes such as semiconductor device fabrication. Notably, the ability of a solid to drive this chemical transformation depends on its position in the Galvanic series. For example, Mg and Al have low oxidation resistance; therefore, they form higher H_2O_2(aq), and, in contrast, Ti and stainless steel have high oxidation resistance, forming a lower amount of H_2O_2(aq). Next, our XPS experiments have revealed that the solid surface gets oxidized during the formation of H_2O_2, which refutes the suggestion that during the formation of H_2O_2 at the solid–water interface, water molecules transfer electrons to the solid, reducing it.[11,15]

Crucially, in the absence of dissolved O_2 in water, $H_2O_2(aq)$ was not observed in pneumatic sprays or in bulk water containing pellets of Mg or Al (down to the 50 nM detection limit). This demonstrates that (i) the air–water interface of sprayed microdroplets and the putative (instantaneous) ultrahigh electric field therein are not capable of spontaneously forming H_2O_2 (Fig. 6), and (ii) the presence of dissolved O_2 is a required condition for the solid–water interface to form H_2O_2. Therefore, we submit that the latest claims[59,64] of the formation of ≤ 3 μM $H_2O_2(aq)$ in water microdroplets (containing dissolved O_2) suffered from artifacts arising due to the unavoidable physical contact of water with solid surfaces (e.g., during sample preparation, collection, and analysis), and evaporative concentration.[48]

When water microdroplets were formed by nebulizing with $O_2(g)$, it increased the $O_2(aq)$ concentration, promoting the formation of $H_2O_2(aq)$ at the solid–water interface. Conversely, if the water is devoid of $O_2(g)$, H_2O_2 is not formed spontaneously at the solid–water interface. In that scenario, the air–water interface can contribute to the H_2O_2 formation in the following two ways: (i) transfer $O_2(g)$ to be reduced at the solid–water interface to form $H_2O_2(aq)$ (see the inset in Fig. 7); or (ii) transfer $O_3(g)$ to oxidize water to form $H_2O_2(aq)$ without the necessity of the solid–water interface. We hope these findings will advance the current knowledge of aquatic chemistry and prove relevant to corrosion science, electrochemistry, and soil chemistry.

Materials and methods

Chemicals

Deionized water was obtained from a Milli-Q Advantage 10 set-up (18.2 MΩ cm resistivity). This study used commercially available 30% hydrogen peroxide (H_2O_2) solution (Sigma-Aldrich CAS no. 7722-84-1) and deuterium oxide ((D_2O, Catalog no. 3000007892).

Spraying microdroplets

Inside a glove box with a controlled $N_2(g)$ atmosphere to prevent ambient contamination, the water was injected using a stainless steel capillary tube with an inner diameter of 100 μm using a syringe pump (PHD Ultra, Harvard Apparatus). Ultra-pure N_2/O_2 was pushed through a coaxial stainless steel sheath with an inner diameter of 430 μm to nebulize the water stream (Fig. S1†). The liquid water flow rate was 25 μL min^{-1}, and approximately 2 ml of microdroplet volume was collected in clean glass vials for further analysis.

Deoxygenation of water

Water was heated in an autoclave to its boiling point, followed by cooling via $N_2(g)$ bubbling for 45 min, lowering the temperature to about 40 °C. An O_2 sensor (WTW Multi 3320) measured the dissolved O_2 concentration in water with a detection limit of 0.01 mg L^{-1}. After this treatment, we could not observe a signal for the $O_2(aq)$, meaning it was below the detection limit. Next, the water was quickly transferred to a glove box filled with N_2 gas, where glass bottles were filled and sealed. The water sealed in an $N_2(g)$ filled glove box was autoclaved at 121 °C for 10 min to remove organic contamination on the vials.

Substrates for condensation

Silicon (SiO_2/Si) wafers of about 300 μm thickness, 10 cm in diameter, and 2 μm-thick thermally grown oxide were purchased from Silicon Valley Microelectronics (Catalog #SV010, p-type and 100 orientation). Fresh Si surfaces were prepared by etching the SiO_2 layer via reactive ion etching (using C_4F_8 and $O_2(g)$ for 5 mi) inside the KAUST cleanroom.[65] Directly afterward, condensation experiments were performed on the etched surfaces, and water samples were collected in clean glass vials for ^{1}H-NMR analysis. Next, the following commercially available plates comprising metals or metallic alloys were used: Mg alloy (AZ31B, Thermo Scientific, Catalog No. AA14066RF), Al (Fisher Scientific, Catalog no. AA42124RF), mild steel, stainless steel (SS304), Zn (Thermo Scientific, Catalog No. AA11914FI), Cu (Thermo Scientific Chemicals, Catalog no. AA43822KS), and Ti (ASTM B 265 Trinity Brand Industries INC part #6T-5). The native oxide on the metal plates was removed via mechanical polishing using SiC emery papers with a grit size of 400 to 1500, followed by cleaning with pressurized N_2 gas. For the condensation experiments, DI water was heated to 60 °C inside a closed chamber to produce the water vapor. Water microdroplets formed on cooled substrates (placed directly on ice) were collected using a low-pressure N_2 gas stream and transferred to NMR tubes and glass vials for further analysis.

Hydrogen peroxide assay kit (HPAK) assay

The H_2O_2 concentration of the condensed water was quantified using the hydrogen peroxide assay kit (Fluorometric-Near Infrared, Catalog # ab138886). It contains a unique AbIR peroxidase indicator that produces fluorescence independent of the solution pH in the range of 4 to 10. Its maximum excitation wavelength is 647 nm, and the maximum emission is 674 nm. The horseradish peroxidase enzyme catalyzes the reaction between H_2O_2 and the indicator and enhances the fluorescence signal. This action facilitates the linear detection range from 30 nM to 10 μM. The calibration curve (Fig. S3†) was realized by adding 50 μL of an H_2O_2 standard solution from a concentration of 50 nM to 10 μM into 50 μL of the H_2O_2 reaction mixture using a black 96-well microtiter-plate, and the SpectraMax M3 microplate reader (Molecular Devices LLC). The analysis software was SoftMax Pro 7. The water microdroplets were analyzed similarly by mixing 50 μL of each sample with the H_2O_2 reaction mixture, obtaining the respective concentration from the calibration curve.

NMR spectroscopy analysis and sample preparation

No chemical was added to adjust the pH of the samples to avoid contamination. In each case, 10 μL of D_2O was added to 490 μL analyte in regular 5 mm quartz NMR tubes for testing. All NMR measurements were conducted on a Bruker 950 MHz Avance Neo NMR spectrometer equipped with a 5 mm Z-axis gradient

TCI cryoprobe at the temperature of 275 K. During the measurement, a 6 ms Gaussian 90° pulse was applied to selectively excite the protons of H_2O_2, followed by a 53 ms acquisition corresponding to 1024 detecting points with a spectral width of 9615 Hz. Over 50 000 scans were collected with a recycle delay of 1 ms between scans. The NMR data were analyzed using TopSpin 4.2.0 software.

XPS measurements

A Kratos Axis Supra instrument equipped with a monochromatic Al Kα X-ray source ($h\nu = 1486.6$ eV) operating at a power of 75 W under UHV conditions in the range of 10^{-9} mbar was used to obtain the data. All spectra were recorded in hybrid mode using magnetic and electrostatic lenses and an aperture slot of 300×700 μm. The high-resolution spectra were acquired at a fixed analyzer pass energy of 20 eV. The adventitious carbon (C 1s) peak at 284.5 eV was used as a reference for calibrating all peaks.

Data availability

All data needed to evaluate the conclusions in the paper are present in the paper or the ESI.†

Author contributions

HM conceived the research plan and oversaw its execution. ME designed and performed the condensation and spray experiments inside the glovebox and collected the ^{1}H-NMR and HPAK data. ME and HM analyzed the data and wrote the manuscript together.

Conflicts of interest

The authors declare no competing interests.

Acknowledgements

References

1 J. A. Otter, S. Yezli, F. Barbut and T. M. Perl, in *Decontamination in Hospitals and Healthcare*, ed. J. Walker, Woodhead Publishing, 2nd edn, 2020, pp. 323–369, DOI: **10.1016/B978-0-08-102565-9.00015-7**.

2 L. Kurti and B. Czakó, *Strategic Applications of Named Reactions in Organic Synthesis*, Academic Press, Illustrated edition, 2005.

3 W. Kopacz, A. Okninski, A. Kasztankiewicz, P. Nowakowski, G. Rarata and P. Maksimowski, Hydrogen peroxide–A promising oxidizer for rocket propulsion and its application in solid rocket propellants, *FirePhysChem*, 2022, **2**, 56–66.

4 M. Ksibi, Chemical oxidation with hydrogen peroxide for domestic wastewater treatment, *Chem. Eng. J.*, 2006, **119**, 161–165.

5 R. Hans-Joachim and P. Georg, Production of hydrogen peroxide, *US Pat.*, US2158525A, 1939.

6 A. T. Murray, S. Voskian, M. Schreier, T. A. Hatton and Y. Surendranath, Electrosynthesis of Hydrogen Peroxide by Phase-Transfer Catalysis, *Joule*, 2019, **3**, 2942–2954.

7 X. Zhang, X. Zhao, P. Zhu, Z. Adler, Z.-Y. Wu, Y. Liu and H. Wang, Electrochemical oxygen reduction to hydrogen peroxide at practical rates in strong acidic media, *Nat. Commun.*, 2022, **13**, 2880.

8 K. Wang, J. Huang, H. Chen, Y. Wang and S. Song, Recent advances in electrochemical 2e oxygen reduction reaction for on-site hydrogen peroxide production and beyond, *Chem. Commun.*, 2020, **56**, 12109–12121.

9 J. K. Lee, K. L. Walker, H. S. Han, J. Kang, F. B. Prinz, R. M. Waymouth, H. G. Nam and R. N. Zare, Spontaneous generation of hydrogen peroxide from aqueous microdroplets, *Proc. Natl. Acad. Sci. U. S. A.*, 2019, **116**, 19294–19298.

10 J. K. Lee, H. S. Han, S. Chaikasetsin, D. P. Marron, R. M. Waymouth, F. B. Prinz and R. N. Zare, Condensing water vapor to droplets generates hydrogen peroxide, *Proc. Natl. Acad. Sci. U. S. A.*, 2020, **117**, 30934–30941.

11 B. Chen, Y. Xia, R. He, H. Sang, W. Zhang, J. Li, L. Chen, P. Wang, S. Guo, Y. Yin, L. Hu, M. Song, Y. Liang, Y. Wang, G. Jiang and R. N. Zare, Water–solid contact electrification causes hydrogen peroxide production from hydroxyl radical recombination in sprayed microdroplets, *Proc. Natl. Acad. Sci. U. S. A.*, 2022, **119**, e2209056119.

12 M. T. Dulay, C. A. Huerta-Aguilar, C. F. Chamberlayne, R. N. Zare, A. Davidse and S. Vukovic, Effect of relative humidity on hydrogen peroxide production in water droplets, *QRB Discov.*, 2021, **2**, e8.

13 M. T. Dulay, J. K. Lee, A. C. Mody, R. Narasimhan, D. M. Monack and R. N. Zare, Spraying Small Water Droplets Acts as a Bacteriocide, *QRB Discov.*, 2020, **1**, e3.

14 C. Zhu and J. S. Francisco, Production of hydrogen peroxide enabled by microdroplets, *Proc. Natl. Acad. Sci. U. S. A.*, 2019, **116**, 19222–19224.

15 Y. Xia, J. Li, Y. Zhang, Y. Yin, B. Chen, Y. Liang, G. Jiang and R. N. Zare, Contact between water vapor and silicate surface causes abiotic formation of reactive oxygen species in an anoxic atmosphere, *Proc. Natl. Acad. Sci. U. S. A.*, 2023, **120**, e2302014120.

16 H. Mishra, S. Enami, R. J. Nielsen, L. A. Stewart, M. R. Hoffmann, W. A. Goddard and A. J. Colussi, Bronsted basicity of the air-water interface, *Proc. Natl. Acad. Sci. U. S. A.*, 2012, **109**, 18679–18683.

17 R. J. Saykally, Air/water interface: Two sides of the acid-base story, *Nat. Chem.*, 2013, **5**, 82–84.

18 A. Gallo, A. S. F. Farinha, M. Dinis, A.-H. Emwas, A. Santana, R. J. Nielsen, W. A. Goddard and H. Mishra, The chemical reactions in electrosprays of water do not always correspond to those at the pristine air–water interface, *Chem. Sci.*, 2019, **10**, 2566–2577.

19 A. J. Colussi and S. Enami, Comment on "The chemical reactions in electrosprays of water do not always correspond to those at the pristine air–water interface" by A. Gallo Jr, A. S. F. Farinha, M. Dinis, A.-H. Emwas, A. Santana, R. J. Nielsen, W. A. Goddard III and H. Mishra, *Chem. Sci.*, 2019, **10**, 2566, DOI: 10.1039/C9SC00991D.

20 A. Gallo, A. S. F. Farinha, A.-H. Emwas, A. Santana, R. J. Nielsen, W. A. Goddard and H. Mishra, Reply to the 'Comment on "The chemical reactions in electrosprays of water do not always correspond to those at the pristine air–water interface"' by A. J. Colussi and S. Enami, 2019, 10, DOI: 10.1039/c9sc00991d, *Chem. Sci.*, 2019, **10**, 8253–8255, DOI: 10.1039/C9SC02702E.

21 J. Nauruzbayeva, Z. Sun, A. Gallo, M. Ibrahim, J. C. Santamarina and H. Mishra, Electrification at water–hydrophobe interfaces, *Nat. Commun.*, 2020, **11**, 5285.

22 Y. Uematsu, D. J. Bonthuis and R. R. Netz, Charged Surface-Active Impurities at Nanomolar Concentration Induce Jones-Ray Effect, *J. Phys. Chem. Lett.*, 2018, **9**, 189–193.

23 S. J. Byrnes, P. L. Geissler and Y. R. Shen, Ambiguities in surface nonlinear spectroscopy calculations, *Chem. Phys. Lett.*, 2011, **516**, 115–124.

24 N. Agmon, H. J. Bakker, R. K. Campen, R. H. Henchman, P. Pohl, S. Roke, M. Thämer and A. Hassanali, Protons and Hydroxide Ions in Aqueous Systems, *Chem. Rev.*, 2016, **116**, 7642–7672.

25 M. F. Ruiz-Lopez, J. S. Francisco, M. T. C. Martins-Costa and J. M. Anglada, Molecular reactions at aqueous interfaces, *Nat. Rev. Chem*, 2020, **4**, 459–475.

26 M. I. Jacobs, R. D. Davis, R. J. Rapf and K. R. Wilson, Studying Chemistry in Micro-compartments by Separating Droplet Generation from Ionization, *J. Am. Soc. Mass Spectrom.*, 2019, **30**, 339–343.

27 G. Rovelli, M. I. Jacobs, M. D. Willis, R. J. Rapf, A. M. Prophet and K. R. Wilson, A critical analysis of electrospray techniques for the determination of accelerated rates and mechanisms of chemical reactions in droplets, *Chem. Sci.*, 2020, **11**, 13026–13043.

28 S. Pullanchery, S. Kulik, B. Rehl, A. Hassanali and S. Roke, Charge transfer across C–H···O hydrogen bonds stabilizes oil droplets in water, *Science*, 2021, **374**, 1366–1370.

29 H. Wei, E. P. Vejerano, W. Leng, Q. Huang, M. R. Willner, L. C. Marr and P. J. Vikesland, Aerosol microdroplets exhibit a stable pH gradient, *Proc. Natl. Acad. Sci. U. S. A.*, 2018, **115**, 7272–7277.

30 A. J. Colussi, Can the pH at the air/water interface be different from the pH of bulk water?, *Proc. Natl. Acad. Sci. U. S. A.*, 2018, **115**, E7887.

31 M. Li, Y. Kan, H. Su, U. Pöschl, S. H. Parekh, M. Bonn and Y. Cheng, Spatial homogeneity of pH in aerosol microdroplets, *Chem*, 2023, **9**, 1036–1046.

32 K. Roger and B. Cabane, Why Are Hydrophobic/Water Interfaces Negatively Charged?, *Angew. Chem., Int. Ed.*, 2012, **51**, 5625–5628.

33 K. Roger and B. Cabane, Uncontaminated Hydrophobic/Water Interfaces Are Uncharged: A Reply, *Angew. Chem., Int. Ed.*, 2012, **51**, 12943–12945.

34 K. C. Jena, R. Scheu and S. Roke, Surface Impurities Are Not Responsible For the Charge on the Oil/Water Interface: A Comment, *Angew. Chem., Int. Ed.*, 2012, **51**, 12938–12940.

35 J. K. Beattie and A. Gray-Weale, Oil/Water Interface Charged by Hydroxide Ions and Deprotonated Fatty Acids: A Comment, *Angew. Chem., Int. Ed.*, 2012, **51**, 12941–12942.

36 D. Ben-Amotz, Electric buzz in a glass of pure water, *Science*, 2022, **376**, 800–801.

37 E. Poli, K. H. Jong and A. Hassanali, Charge transfer as a ubiquitous mechanism in determining the negative charge at hydrophobic interfaces, *Nat. Commun.*, 2020, **11**, 901.

38 S. Enami, H. Mishra, M. R. Hoffmann and A. J. Colussi, Protonation and Oligomerization of Gaseous Isoprene on Mildly Acidic Surfaces: Implications for Atmospheric Chemistry, *J. Phys. Chem. A*, 2012, **116**, 6027–6032.

39 J. A. Otter, S. Yezli, F. Barbut and T. M. Perl, An overview of automated room disinfection systems: When to use them and how to choose them, *Decontamination in Hospitals and Healthcare*, 2020, pp. 323–369, DOI: 10.1016/B978-0-08-102565-9.00015-7.

40 K. Li, Y. Guo, S. A. Nizkorodov, Y. Rudich, M. Angelaki, X. Wang, T. An, S. Perrier and C. George, Spontaneous dark formation of OH radicals at the interface of aqueous atmospheric droplets, *Proc. Natl. Acad. Sci. U. S. A.*, 2023, **120**, e2220228120.

41 T. Kakeshpour, B. Metaferia, R. N. Zare and A. Bax, Quantitative detection of hydrogen peroxide in rain, air, exhaled breath, and biological fluids by NMR spectroscopy, *Proc. Natl. Acad. Sci. U. S. A.*, 2022, **119**, e2121542119.

42 S. Lin, L. N. Y. Cao, Z. Tang and Z. L. Wang, Size-dependent charge transfer between water microdroplets, *Proc. Natl. Acad. Sci. U. S. A.*, 2023, **120**, e2307977120.

43 H. Xiong, J. K. Lee, R. N. Zare and W. Min, Strong Electric Field Observed at the Interface of Aqueous Microdroplets, *J. Phys. Chem. Lett.*, 2020, **11**, 7423–7428.

44 H. Hao, I. Leven and T. Head-Gordon, Can electric fields drive chemistry for an aqueous microdroplet?, *Nat. Commun.*, 2022, **13**, 280.

45 J. P. Heindel, H. Hao, R. A. LaCour and T. Head-Gordon, Spontaneous formation of hydrogen peroxide in water microdroplets, *J. Phys. Chem. Lett.*, 2022, **13**, 10035–10041.

46 A. J. Colussi, Mechanism of Hydrogen Peroxide Formation on Sprayed Water Microdroplets, *J. Am. Chem. Soc.*, 2023, **145**, 16315–16317.

47 N. H. Musskopf, A. Gallo, P. Zhang, J. Petry and H. Mishra, The Air–Water Interface of Water Microdroplets Formed by Ultrasonication or Condensation Does Not Produce H2O2, *J. Phys. Chem. Lett.*, 2021, **12**, 11422–11429.

48 A. Gallo Jr, N. H. Musskopf, X. Liu, Z. Yang, J. Petry, P. Zhang, S. Thoroddsen, H. Im and H. Mishra, On the formation of hydrogen peroxide in water microdroplets, *Chem. Sci.*, 2022, **13**, 2574–2583.

49 D. Nguyen and S. C. Nguyen, Revisiting the Effect of the Air–Water Interface of Ultrasonically Atomized Water Microdroplets on H2O2 Formation, *J. Phys. Chem. B*, 2022, **126**, 3180–3185.

50 D. Nguyen, P. Lyu and S. C. Nguyen, Experimental and Thermodynamic Viewpoints on Claims of a Spontaneous H2O2 Formation at the Air–Water Interface, *J. Phys. Chem. B*, 2023, **127**, 2323–2330.

51 M. T. Martins-Costa and M. F. Ruiz-López, Probing solvation electrostatics at the air–water interface, *Theor. Chem. Acc.*, 2023, **142**, 29.

52 M. Peplow, Claims of water turning into hydrogen peroxide spark debate, *Chem. Eng. News*, 2022, https://cen.acs.org/research-integrity/reproducibility/Claims-water-turning-hydrogen-peroxide/100/web/2022/05.

53 T. Cozens, Study casts doubt on water microdroplets' ability to spontaneously produce hydrogen peroxide, *Chem. World*, 2022, https://www.chemistryworld.com/news/study-casts-doubt-on-water-microdroplets-ability-to-spontaneously-produce-hydrogen-peroxide/4015169.article.

54 R. Trager, Water surprise: microdroplets have potential to produce hydrogen peroxide, *Chem. World*, 2019, https://www.chemistryworld.com/news/water-surprise-microdroplets-have-potential-to-produce-h2o2/3010950.article#commentsJump.

55 P. Riesz, D. Berdahl and C. L. Christman, Free radical generation by ultrasound in aqueous and nonaqueous solutions, *Environ. Health Perspect.*, 1985, **64**, 233–252.

56 X. Fang, G. Mark and C. von Sonntag, OH radical formation by ultrasound in aqueous solutions Part I: the chemistry underlying the terephthalate dosimeter, *Ultrason. Sonochem.*, 1996, **3**, 57–63.

57 M. Hoffmann, I. Hua and R. Hoechemer, Application of Ultrasonic Irradiation for the Degradation of Chemical Contaminants in Water, *Ultrason. Sonochem.*, 1996, **3**, 168–172.

58 J. H. Bang and K. S. Suslick, Applications of Ultrasound to the Synthesis of Nanostructured Materials, *Adv. Mater.*, 2010, **22**, 1039–1059.

59 M. A. Mehrgardi, M. Mofidfar and R. N. Zare, Sprayed Water Microdroplets Are Able to Generate Hydrogen Peroxide Spontaneously, *J. Am. Chem. Soc.*, 2022, **144**, 7606–7609.

60 T. Kakeshpour and A. Bax, NMR characterization of H2O2 hydrogen exchange, *J. Magn. Reson.*, 2021, **333**, 107092.

61 M. Hayyan, M. A. Hashim and I. M. AlNashef, Superoxide Ion: Generation and Chemical Implications, *Chem. Rev.*, 2016, **116**, 3029–3085.

62 A. J. Bard and L. R. Faulkner, *Electrochemical Methods: Fundamentals and Applications*, John Wiley & Sons, 2nd edn, 2001.

63 I. Ivanovic-Burmazovic, Catalytic dismutation vs. reversible binding of superoxide, *Adv. Inorg. Chem.*, 2008, **60**, 59–100.

64 K. Zhou, H. Su, J. Gao, H. Li, S. Liu, X. Yi, Z. Zhang and W. Wang, Deciphering the Kinetics of Spontaneous Generation of H2O2 in Individual Water Microdroplets, *J. Am. Chem. Soc.*, 2024, DOI: 10.1021/jacs.3c09864.

65 S. Arunachalam, E. M. Domingues, R. Das, J. Nauruzbayeva, U. Buttner, A. Syed and H. Mishra, Rendering SiO2/Si Surfaces Omniphobic by Carving Gas-Entrapping Microtextures Comprising Reentrant and Doubly Reentrant Cavities or Pillars, *J. Vis. Exp.*, 2020, e60403, DOI: 10.3791/60403.